

A singlet state oxygen generation model based on the Monte Carlo method of visible antibacterial blue light inactivation

Wanqing Zhang ^a, Ping Su ^a, Jianshe Ma ^{a,*}, Mali Gong ^{a,b}, Liya Ma ^c, Jing Wang ^d

^a Tsinghua Shenzhen International Graduate School, Tsinghua University, Shenzhen 518055, China

^b Department of Precision Instrument, Tsinghua University, Beijing 100084, China

^c Shenzhen Baan Women and Children's Hospital, Jinan University, Shenzhen 518100, China

^d College of Water Conservancy, Yunnan Agricultural University, Kunming 650000, China



ARTICLE INFO

Keywords:

Visible antibacterial blue light
Antibacterial photodynamic treatment
Monte Carlo simulation
Mathematical model

ABSTRACT

Visible antibacterial blue light (VABL) has received much attention recently as a nondestructive inactivation approach. However, due to the sparse distribution of bacteria, the light energy evaluation method used in existing studies is inaccurate. Thus, the sensitivity of microorganisms to VABL in different experiments cannot be compared. In this paper, a Monte Carlo-based photon transport model with the optimized scattering phase function was constructed. The model calculated the spatial light energy distribution and the temporal distribution of cumulative singlet state oxygen (CSO) under various cell and medium parameters. The simulation results show that when the cells are sparsely distributed, <30% of light energy from the light source is absorbed by microbes and participates in photochemical reactions. The CSO produced increases with cell density and cell size. Little light energy is available, and thus, the concentration of CSO produced is insufficient to inactivate microbes at deeper depths. As the light intensity and inactivation time increased, the production of singlet state oxygen tended to level off. The model proposed here can quantify the generation of singlet state oxygen and provide a more accurate light energy guide for the VABL inactivation process.

1. Introduction

Light energy-based inactivation techniques can inactivate a wide range of pathogens without reducing any antibiotic resistance, which has become a potential approach in the context of pandemic outbreaks [1–3]. Among these techniques, visible antibacterial blue light (VABL) has received much interest in recent years due to its safety for organisms [4,5]. Blue light has been shown to inactivate microbes or tumor cells in the presence of exogenous photosensitizers (PS) and oxygen, which is called photodynamic treatment (PDT). Researchers have proposed that oxygen-independent photoinactivation (Type III photochemical pathway) can also kill microorganisms [6]. While for the principle of VABL-based inactivation, it is generally accepted that some endogenous PS, such as porphyrins and flavins [7], can absorb light energy and convert some substances into reactive oxygen species (ROS), which would subsequently inactivate bacteria [8,9].

The complicated photochemical reactions in VABL inactivation generating ROS are mainly driven by light energy, the concentration of surrounding oxygen [10,11], and the concentration of endogenous PS

[12]. Depending on whether it is photoinduced electron transfer or energy transfer, ROS can be classified as type I and type II [13]. Singlet state oxygen is the type II ROS produced by excited triplet state PS and molecular oxygen [14]. According to previous studies, singlet state oxygen is considered the main inactivating substance in VABL inactivation [15,16]. Therefore, the generation of singlet state oxygen is significant for VABL inactivation.

In practical applications, VABL is used in environmental disinfection [17,18] and the sterilization of food such as fruits and vegetables [19]. In addition, a large number of in vivo studies have also demonstrated the nondestructive effect of VABL on host cells, which means that VABL has great potential for skin disinfection and other medical applications [20–23]. In terms of theoretical research, a considerable number of studies have explored the inactivation effect of VABL and built models of light dose and bacterial reduction [24–26]. However, the current model is mainly fitted by the experimental results under different light doses instead of the mechanism of VABL inactivation. The traditional models of inactivation kinetics, including the modified Chick–Watson model [27], Weibull model [28], and Hom model [27], can precisely fit the

* Corresponding author.

E-mail address: ma.jianshe@sz.tsinghua.edu.cn (J. Ma).

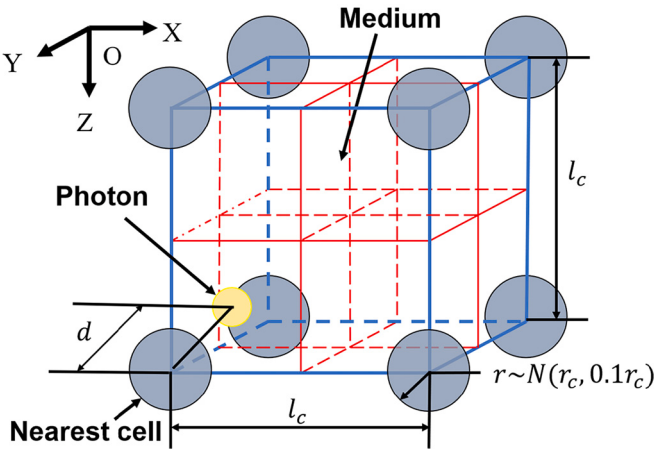


Fig. 1. The cell spatial arrangement model.

experimental results by some parameters that lack physical significance [29]. However, the lack of mechanistic studies on the VABL inactivation process makes it difficult to accurately compare the results between different studies.

In the field of PDT of tumors, the transmission of light energy in tissues and the production of ROS are considered to be important factors affecting the treatment [30,31]. Analogous to the PDT of tumors, VABL inactivation should also build a mechanistic model and explore the parameters that influence the effect. Theoretically, VABL inactivation can be divided into three continuous and parallel processes. The first process is called the light energy transfer model, which describes the process by which the light source launches and transfers energy into microbes. Then, the photochemical reaction model shows the process by which the light energy reacts with PS as a reactant. Finally, the threshold lethal model defines the threshold concentration of ROS that inactivate microorganisms.

Most existing studies ignore the first process. The light energy is evaluated by the energy emitted from the light source (i.e., electrical energy) or the energy measured by an energy meter at the same distance [32–35]. However, due to the sparse distribution of bacteria, a large part of the light energy is absorbed by the culture medium or leaves the photobioreactor through transmission and reflection. The above-mentioned energy is not the actual energy involved in the photochemical reaction. With the development of the VABL inactivation field, an increasing number of studies have realized that ROS, especially singlet state oxygen, generation is the result of the inactivation effect of VABL [15,21]. As the most important toxic substance, the quantitative calculation and detection of singlet state oxygen is helpful to better design an inactivated light source with environmental parameters and lay the foundation of the lethal threshold model.

The contributions of this work are three folds. Firstly, a Monte Carlo-based photon transport model with the optimized scattering phase function was constructed. Under different bacterial cell parameters and medium environment parameters, the efficient light energy distribution for a given light source energy was obtained by the model. Secondly, a mathematical model of the photochemical kinetics of VABL inactivation in the case of bacterial inactivation based on singlet state oxygen was established. Finally, a complete generation model of the singlet state oxygen induced by light source energy was developed and the distribution of cumulative singlet state oxygen concentration with inactivation time was obtained. To the best of our knowledge, no such model has been developed to explore the transmission of light source energy during the inactivation process and quantify the relation between the light source energy and the intracellular singlet state oxygen generation under various parameters in VABL inactivation. Our work explains the differences in inactivation doses from the perspective of light energy under the experimental conditions in different studies and develops a mechanistic model to help guide the future practical application of VABL.

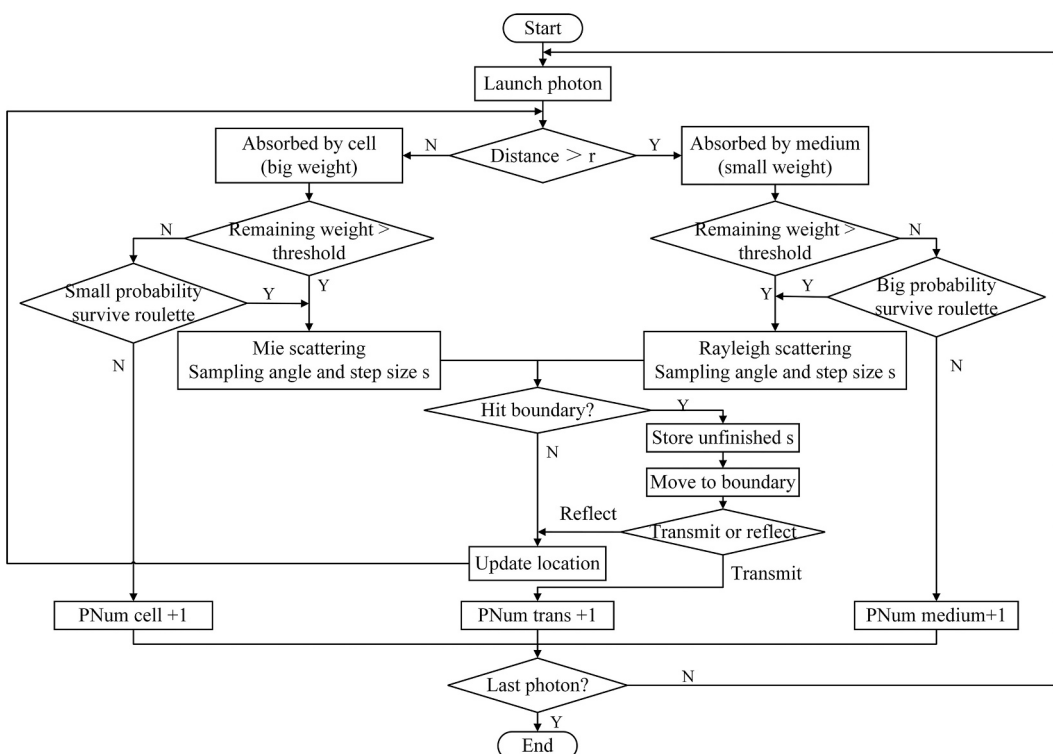


Fig. 2. Simulation process of the photon path in SPR.

2. Methods

2.1. Cell Spatial Arrangement Model in a Simulated Photobioreactor

The simulative photobioreactor (SPR) was set to be an infinite space consisting of uniformly distributed random Gaussian spherical bacterial cells and medium, as shown in Fig. 1. It was infinitely large in the XOY plane. An upper boundary $z = 0$ mm and a lower boundary $z = 3$ mm were set to better fit the actual experimental situation. Although the true shapes of bacteria are diverse [36], the shape of the cell can be considered a sphere whose radius r obeys a normal distribution $N(r_c, 0.1r_c)$ because of their sparse distribution. According to the general volume of the bacteria, r_c was taken in the range of 0.5–3.5 μm [37]. The distance between adjacent cells was defined as l_c . l_c corresponds to the cell density as defined in Eq. (1).

$$l_c = 10 \times \sqrt[3]{1/\text{cell density}} \quad (1)$$

where *cell density* is in units of cells/cm^3 and l_c is in units of mm.

2.2. Monte Carlo-Based Photon Transport Model in a Simulated Photobioreactor

The propagation of light in the SPR is determined by the radiation transport equation. The Monte Carlo (MC) method is proven to be an exact approximation approach to solve the equation if a sufficient number of “photons” (stands for unit energy) is emitted [38]. Different from the MC model in tissue optics [39], the transmission of light in SPR needs to be classified because different types of scattering obey different scattering phase functions. In the cell, Mie scattering occurs because the cell size is close to the wavelength of VABL. In the medium environment, light undergoes Rayleigh scattering.

The MC-based photon transport model in SPR was established as shown in Fig. 2. For each step of the path of a photon, the Euclidean distance d between the current position of the photon and the nearest cell was compared with the cell radius r (shown in Fig. 1). It determines the weight loss of the photon and the type of scattering in the step. Similarly, a “survive roulette” term was also introduced in the model to terminate the photon in a more rational manner. Since the photon undergoes a photochemical reaction inside the cell, a higher survival roulette factor was set to the photon dead inside the cell.

In this paper, μ_t^m and μ_t^c were used to characterize the ability of the medium and the cell to attenuate the light energy, as shown in Eq. (2).

$$\mu_t^m = \mu_a^m + \mu_s^m \quad (2a)$$

$$\mu_t^c = \mu_a^c + \mu_s^c \quad (2b)$$

where μ_a^m and μ_a^c denote the medium and cell absorption coefficients respectively, in units of mm^{-1} ; μ_s^m and μ_s^c denote the medium and cell scattering coefficients respectively. p_m and p_c were used to characterize the absorption ability of the medium and the cell, as shown in Eq. (3).

$$p_m = \mu_a^m / \mu_t^m \quad (3a)$$

$$p_c = \mu_a^c / \mu_t^c \quad (3b)$$

The initial weight of each photon was set to 1. The energy distribution in the SPR for a given light source energy was obtained by recording the ratio of the weights carried by the three types of photons. As shown in Fig. 2, the “PNum cell” was the number of photons absorbed by the cell. The “PNum medium” was the number of photons absorbed by the medium. The “PNum trans” was the number of photons that left the SPR. The maximum light source energy that can be absorbed by the cells in the system can be defined as

$$\frac{\text{PNum cell}}{\text{Total number of photons}} \times \text{light source energy}$$

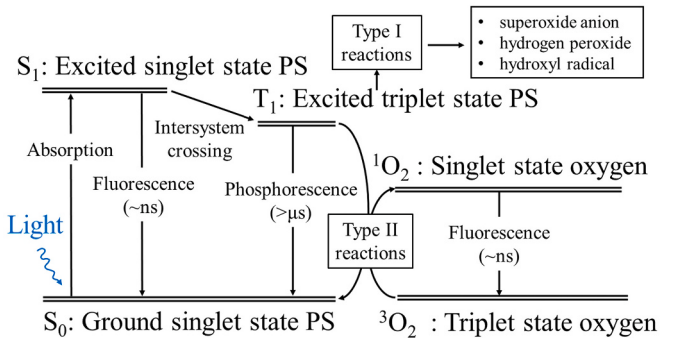


Fig. 3. Jablonski diagram.

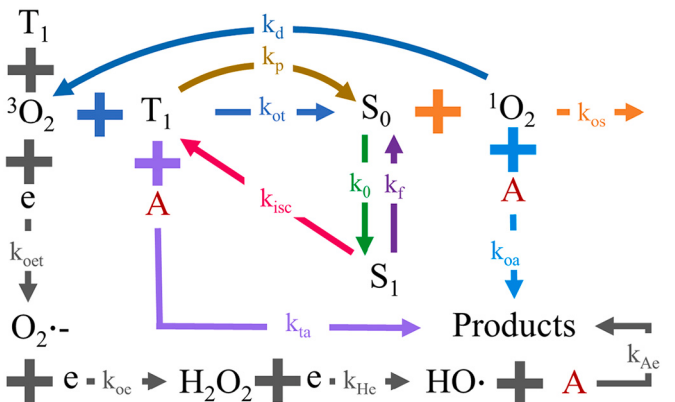


Fig. 4. Photochemical reactions.

All experiments in this paper used a light source intensity set to 100 mW/cm^2 , and the total number of photons was 10^6 .

2.3. Optimized Scattering Phase Function Based on the Particle Swarm Optimization

The two-term Henyey-Greenstein phase function (TTHG) [40,41] was used in this paper to the sample angle in the MC simulation. Compared with the Henyey-Greenstein phase function (HG), the TTHG can better fit the backwards Mie scattering. The TTHG is defined by Eq. (4).

$$P_{TTHG}(\theta) = \alpha \cdot \frac{1 - g_a^2}{(1 - 2g_a \cos\theta + g_a^2)^{3/2}} + (1 - \alpha) \cdot \frac{1 - g_b^2}{(1 - 2g_b \cos\theta + g_b^2)^{3/2}} \quad (4)$$

where g_a and g_b are two asymmetric factors representing the forwards and backwards scattering, and α is the weight. These three parameters are difficult to determine by calculation. Thus, the particle swarm optimization (PSO) algorithm was used to optimize α , g_a , and g_b simultaneously. Other parameters of the PSO algorithm are defined in Appendix A. The objective function was the mean square error of TTHG and Mie scattering approximated at all angles, as shown in Eq. (5).

$$\sigma_{rms} = \sqrt{\frac{\sum_0^\pi [P_{TTHG}(\theta) - P_{Mie}(\theta)]^2}{n}} \quad (5)$$

According to the principle of Mie scattering, the scattering influencing factors include wavelength, cell size and density, absorption coefficient, and scattering coefficient [42]. The PSO-based TTHG can optimally fit the Mie scattering function dynamically under different parameters and improve the accuracy of the MC-based photon transport

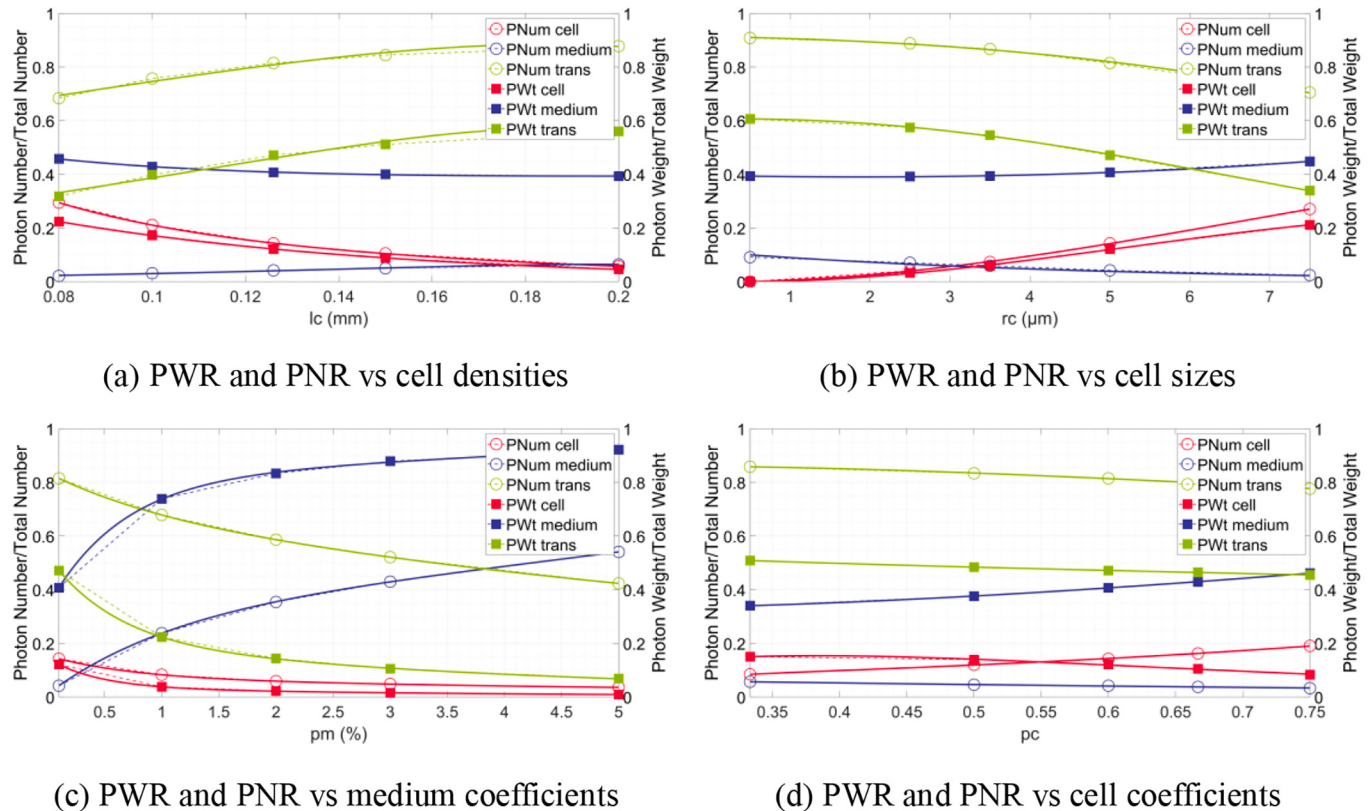


Fig. 5. PWR distribution and PNR distribution for different parameters. “PWT cell” was the summation of the weight of “PNum cell”. The same is true for the other two parameters. All quantities were normalized by dividing by the total number of photons (total weight), i.e., 10^6 .

model.

2.4. Mathematical Description of the Photochemical Kinetics Generating Singlet State Oxygen

The photochemical reactions of VABL inactivation are shown in Fig. 3 and Fig. 4. There are two types of photochemical reactions. In type I processes, the excited triplet state PS T_1 participates in electron transfer and subsequently generates superoxide anion (O_2^-), hydrogen peroxide (H_2O_2), hydroxyl radical ($HO\cdot$). In type II processes, the triplet state oxygen 3O_2 is excited by T_1 and changes to the singlet state oxygen 1O_2 . Although both 1O_2 and $HO\cdot$ show hazards to microbial cells [6], 1O_2 is the main toxic substance in VABL inactivation [43]–[45]. Therefore, the type II reactions generating singlet state oxygen are discussed here.

Fig. 4 shows the conversion relationships and the corresponding reaction rates. According to photochemical kinetics, the rather complex set of differential equations describing the above reactions in type II processes can be simplified to Eqs. (6) and (7). Since the lethal effect of singlet state oxygen is reflected at the cumulative concentration, the concentration of cumulative singlet state oxygen (CSO) was used as the output of the model. The original set of differential equations is shown in Appendix B, which considered and modified the intratumor PDT process proposed by Lopez et al. [38] and the intraskin PDT process proposed by Liu et al. [46].

$$\frac{d[S_0]}{dt} = \frac{-\kappa}{\gamma + \beta + [^3O_2]} \bullet \Phi \bullet [S_0] \bullet \left[\gamma + \frac{\xi\omega\eta S_\Delta [^3O_2]}{S_\Delta\kappa + \xi\omega\eta \bullet [S_0]} \bullet [S_0] \right] \quad (6)$$

$$\frac{d[^1O_2]_{rx}}{dt} = f\kappa \bullet \Phi \bullet [S_0] \bullet \frac{S_\Delta [^3O_2] / \gamma + S_\Delta\kappa / \xi + \omega\eta \bullet [S_0]}{[(\beta + [^3O_2]) / \gamma + 1] \bullet (S_\Delta\kappa / \xi + \omega\eta \bullet [S_0])} \quad (7)$$

where $[S_0]$ is the concentration of ground singlet state PS in units of μM . $[^1O_2]_{rx}$ is the concentration of CSO in units of μM . $[^3O_2]$ is the concentration of triplet state oxygen (i.e., the concentration of ambient oxygen), in units of μM . Φ is the light intensity obtained by the MC model described in Section 2.2 in units of W/cm^2 . The other symbols appearing in the above equation are summarized and defined in Appendix B and Appendix C.

3. Results

3.1. Photon Weight Ratio Distribution and Photon Number Ratio Distribution

The results in this section show the photon weight ratio distribution (PWR) and the photon number ratio distribution (PNR) of the three types of photons under different parameters. The PWR represents the ratio of cell-absorbed light energy, medium-absorbed light energy, and transmitted light energy in the light source energy respectively. In other words, with PWR, we can indirectly measure the amount of cell-absorbed light energy through the easily measured transmitted light energy or light source energy.

As shown in Fig. 5, the number of photons absorbed by the cell and the weight of the photons were relatively close to each other at all parameters. For transmitted photons, the ratio of photon number was greater than the ratio of weight. This result indicated that light energy has a higher probability of being transmitted away. In contrast, the weight ratio of photons absorbed by the medium was much larger than the number ratio, indicating that the photons lose a large amount of energy in the medium. However, in general, medium-absorbed light energy and transmitted light energy occupy most of the light source energy.

As l_c increased and r_c decreased, the photons absorbed by the cells

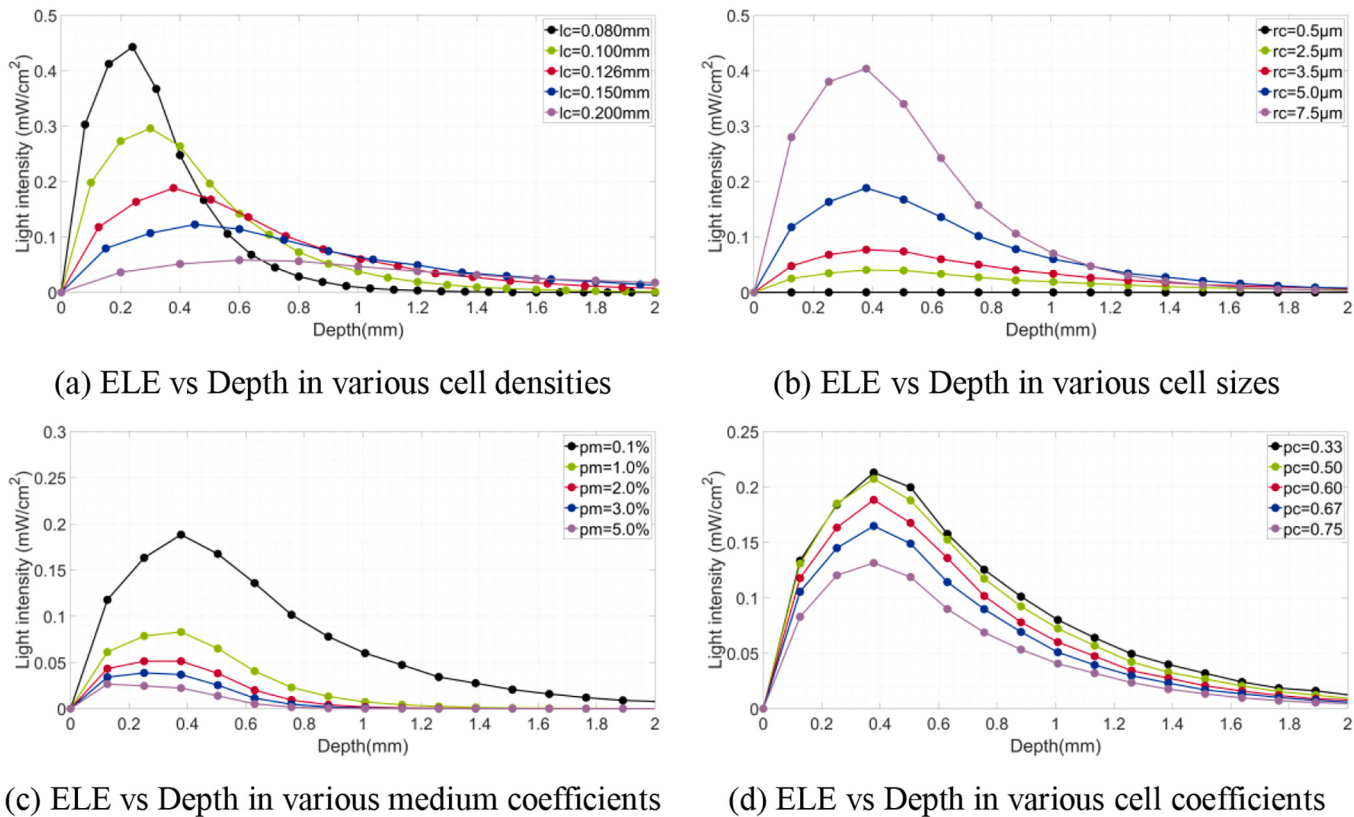


Fig. 6. ELE-Depth distribution for different parameters.

decreased both in number and weight (Fig. 5(a) and (b)). When $l_c = 0.1$ mm and $r_c = 10 \mu\text{m}$, the weight ratio of light energy absorbed by the cells in the whole SPR was only 17.29% of the total weight (Fig. 5(b)). This meant that the remaining 82.71% of the energy was absorbed by the medium or directly emitted out of the SPR. Meanwhile, the PNR was only 21.14%, which is the maximum possible energy absorption of the bacterial cells at this parameter as a percentage of the total energy of the light source. At all densities and sizes in this simulation, the maximum possible energy absorption of the bacterial cells was below 30%.

Fig. 5(c) illustrates that the medium coefficient has less effect on the light energy absorbed by cells. It mainly changed the ratio of whether the light energy was dissipated in the medium or left the SPR. As p_m increased, more energy was absorbed by the medium rather than leaving the SPR. Fig. 5(d) demonstrates that changing the cell coefficient had less effect on the energy distribution. Interestingly, the curves of PWR and PNR of cells crossed each other. As p_c increased, the photons terminating inside the cell and leaving the SPR decreased, while the weight of the photons absorbed by the medium increased. This may be because p_c changes the distribution of the scattering function, which has a larger influence compared to the weight that cells absorb. Therefore, the number of photon's steps in the SPR increases.

3.2. Efficient Light Energy-Depth Distribution

In SPR, the energy absorbed by the cell is the efficient light energy (ELE). ELE is the energy that participates in photochemical reactions and produces ROS. Fig. 6(a) shows that the ELE-Depth distribution increases and then decreases for the same l_c with increasing depth. This trend is consistent with the light energy transmission in the tissue simulation [38,47]. As l_c decreased, the peak of the distribution increased, and the location of the peak appeared at a more superficial layer. For example, for $l_c = 0.08$ mm, the peak occurs at Depth = 0.44 mm, while for $l_c = 0.2$ mm, Depth = 0.62 mm. At the same time, the distribution in SPR with a

smaller l_c exhibited a more rapid decay, which means that less light energy is available to the deeper cells.

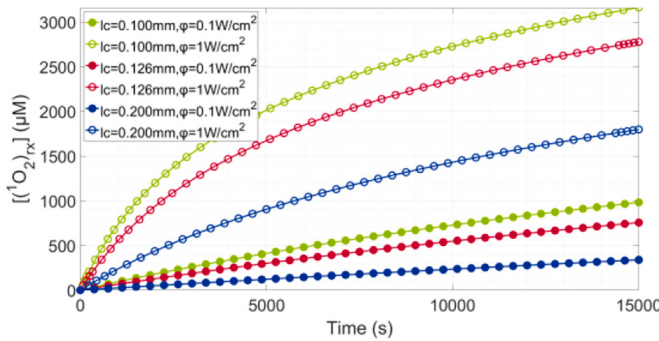
Cell size affects the probability of the ELE-Depth distribution from another aspect. Moreover, cell size affects the parameters of TTHG as well (shown in Section 3.4). Fig. 6(b) demonstrates the ELE-Depth distribution for different cell sizes when the cell density is 5×10^5 cells/cm³ (i.e., $l_c = 0.126$ mm). For the same r_c , the trend of ELE was consistent with Fig. 6(a), which also increased and then decreased. The peak of the distribution remained essentially constant with increasing cell size and was located near Depth = 0.378 mm. r_c does not cause more rapid decay of the ELE-Depth distribution.

Absorption properties of the medium will affect the proportion of light energy absorbed by the medium in SPR. Fig. 6(c) displays the variation of in the ELE-Depth distribution for different medium absorption coefficients. As the value of p_m increased, less energy was absorbed by the cells. The higher the p_m value was, the faster the light energy decayed. This implies that the cells located in deeper layers will not be able to produce sufficient amounts of ROS in an SPR with a medium that has higher absorption coefficients.

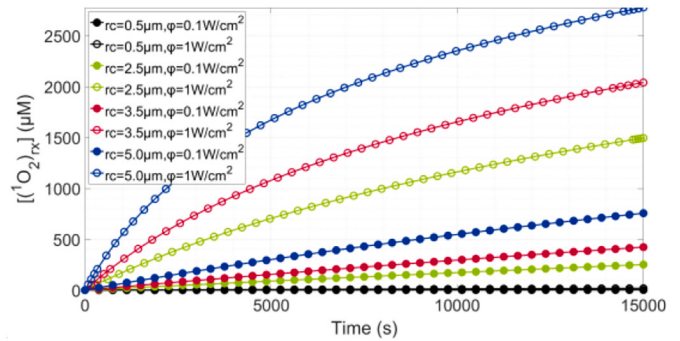
The absorption and scattering coefficients of the cells also affect the transmission of the light energy not only affecting the weight that cells absorbed but also the distribution of the Mie scattering phase function. Fig. 6(d) indicates the ELE-Depth distribution at different p_c . p_c did not change the shape of the ELE distribution, nor did r_c . The depth at which the peak appeared was consistent with different p_c . Interestingly, the ELE at all depths decreased as p_c increased.

3.3. CSO Concentration-Time Distribution

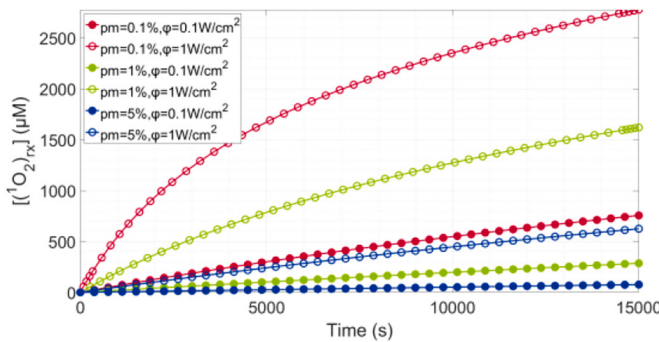
In this section, we focused on the variation in the total CSO concentration produced in SPR with time under different parameters at two light source intensities ($\Phi_{0,1} = 0.1 \text{ W/cm}^2$ and $\Phi_1 = 1 \text{ W/cm}^2$). For the SPR with a light source intensity of 0.1 W/cm^2 , the CSO concentration over time



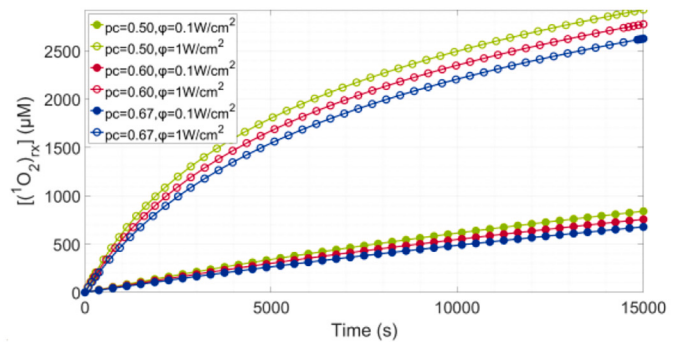
(a) CSO vs Time in various cell densities



(b) CSO vs Time in various cell sizes



(c) CSO vs Time in various medium coefficients



(d) CSO vs Time in various cell coefficients

Fig. 7. CSO concentration vs Time under different parameters.

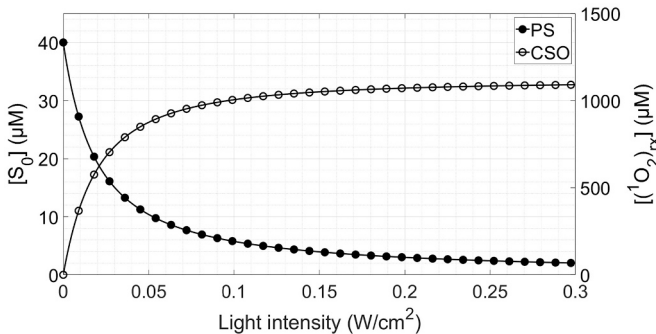


Fig. 8. Marginal effects of light intensity on PS bleaching and CSO generation.

tended to be more linear, and when the light intensity increased to 1 W/cm^2 , the CSO concentration over time showed a nonlinear relationship.

See Fig. 7, for smaller cell densities and smaller cell sizes, the effect of light intensity enhancement is more prominent. At $t = 3000\text{ s}$, the CSO concentration produced by Φ_1 was 5.91 times higher than that of $\Phi_{0.1}$ at $l_c = 0.1\text{ mm}$. At $l_c = 0.2\text{ mm}$, the multiplier was 8.30. With increasing reaction time ($t = 15,000\text{ s}$), the value decreased to 3.22 and 5.29, respectively. Similarly, for $r_c = 2.5\mu\text{m}$, the concentration of CSO generated by Φ_1 was 8.68 times higher than that of $\Phi_{0.1}$ at $t = 3000\text{ s}$. For $r_c = 5\mu\text{m}$, the value was 6.60. For $t = 15,000\text{ s}$, the values were 5.94 and 3.67, respectively. It indicates that with increasing reaction time, the rate of CSO generation starts to weaken. For the SPR with $r_c = 0.5\mu\text{m}$, the generated CSO was very limited even if the light intensity increased 10-fold. This is mainly because the light energy absorbed by the cells is very small at such a cell density. The effect of light intensity on SPR enhancement was higher than that of p_m enhancement. A 10-fold increase in light intensity resulted in a 5.66-fold increase in CSO, while p_m

only resulted in a 2.64-fold increase in CSO. The results suggest that for a medium with higher absorption, the use of higher light intensity resulted in more effective inactivation compared to a diluted ambient medium. Consistent with the aforementioned distribution of ELE, the CSO produced by different p_c was close.

3.4. Marginal Effects of Light Intensity on Photosensitizer Bleaching and CSO Generation

There is a marginal effect of light intensity on the conduct of photochemical reactions. The curves in Fig. 8 represent the relation of light intensity with PS bleaching and CSO generation at time = 1000 s. As the light intensity increased, $[S_0]$ decreased rapidly at first. Correspondingly, the concentration of CSO was generated rapidly. As the light intensity continued to increase, the curve showed an inflection point. When the light intensity was stronger than 0.05 W/cm^2 , the bleaching rate of the PS decreased, which also led to a weakening of the rate of CSO generation.

In addition, the photochemical reaction takes time. As shown in Fig. 8, when the intensity increased, $[S_0]$ did not decay to 0, and residuals still existed. This indicates that the reaction time cannot be compressed to an ultrashort value by a very large light intensity. The CSO curves in Fig. 8 illustrate that the main limitation of CSO generation was the light intensity before the light intensity was saturated. When the light intensity was stronger than the inflection point, the main limiting factor was $[S_0]$. Therefore, we deduce that if it is desired to produce more CSO to achieve sufficient inactivation, increasing the light intensity requires the addition of exogenous photosensitizers.

3.5. Optimized TTHG Fitting Mie Scattering

Figuer 9 shows the results of the TTHG fitting Mie scattering with different parameters. The particle size had a larger influence on the

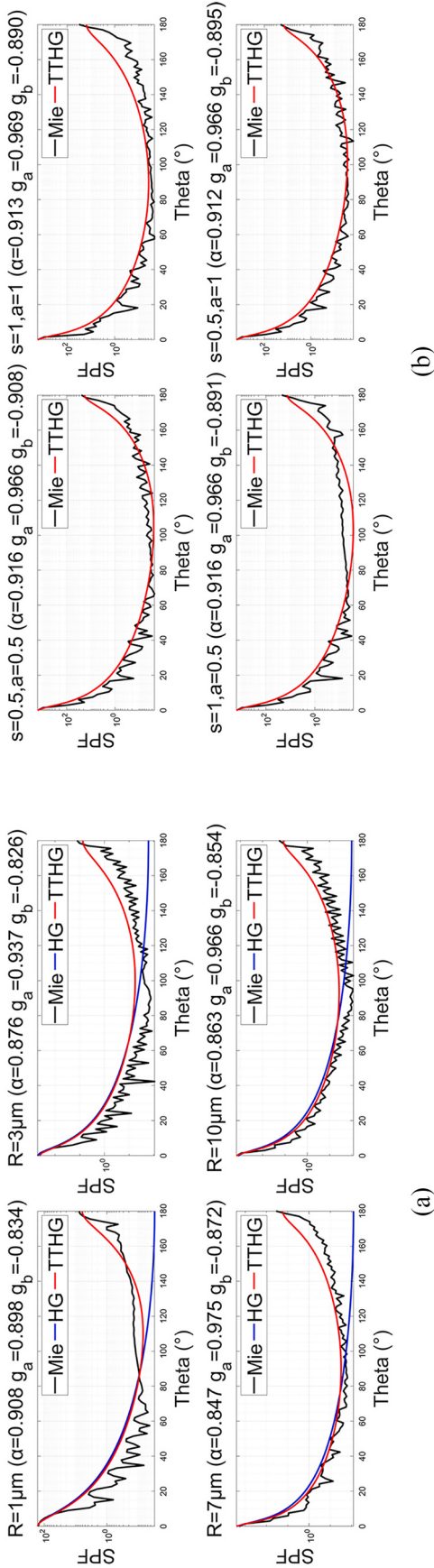


Fig. 9. Comparison of three types of scattering phase functions (SPF).

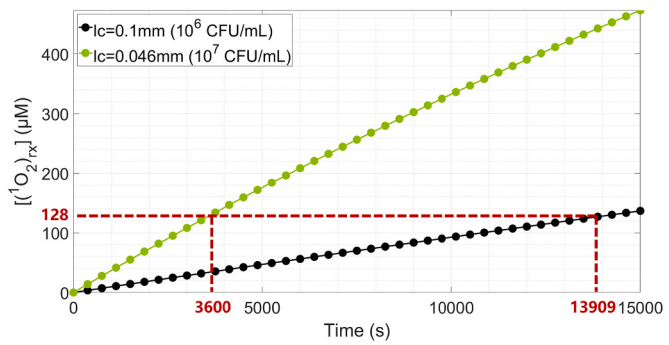


Fig. 10. Simulation of CSO concentration vs Time in the two experiments.

parameters of the TTHG (Fig. 9(a)), while the scattering coefficients s and absorption coefficients a did not contribute to the parameters significantly (Fig. 9(b)). In addition, Fig. 9(a) compares the fitting effects of TTHG and HG on Mie scattering in backscattering (90° – 180°). For backscattering, the phase function of Mie scattering rose, while the HG function continued to fall. This will lead to a very low probability of backscattering when sampling the scattering angle, which produces errors. In contrast, the TTHG based on the PSO algorithm provided an optimal fit to the Mie scattering in the full domain, which demonstrates the superiority of the TTHG function.

4. Discussion

The exorbitant evaluation of light energy in existing studies is too negative to estimate the inactivation of VABL. In fact, the energy involved to achieve the same level of colony-forming unit (CFU) reduction is much lower than the values provided in these papers. On the other hand, these incorrectly estimated light doses cannot serve as a quantitative guide for practical bactericidal applications. This study began with an optimized MC-based photon transport model in SPR that consisted of bacterial cells and a medium. The distribution of CSO concentration with inactivation time was obtained under various cell parameters and medium parameters. Compared to traditional inactivation kinetic equations, our model can quantify the ELE of a given light source energy and the singlet state oxygen concentration from a theoretical perspective. This will improve the current energy evaluation for VABL inactivation of bacteria, which will help to promote the practical application of VABL in a wide variety of mediums (e.g., juice [24], milk [48], plasma [49], etc.).

One of the main contributions of our work is the ability to explain the differences in inactivation doses for the same microbes in different studies. For *Staphylococcus aureus* inactivation, reference [32] achieved a $5 \log_{10}$ CFU reduction at a dose of 36 J/cm^2 , while reference [29] achieved a $4 \log_{10}$ CFU reduction at a dose of 306 J/cm^2 . The main reason that reference [29] achieved a similar reduction at an 8.5-fold dose is mainly due to the difference in cell density. The initial cell density was 10^7 CFU/mL in reference [32] and 10^6 CFU/mL in reference [29]. It agrees well with the simulation results of our model. The CSO generated in SPR can be calculated by the cell density $l_c = 0.1 \text{ mm}$ (corresponding to 10^6 CFU/mL) and $l_c = 0.046 \text{ mm}$ (corresponding to 10^7 CFU/mL). Light intensity of 10 mW/cm^2 and 21 mW/cm^2 were used in the two experiments. According to the conversion relation between light energy and light intensity:

$$E (\text{J/cm}^2) = I (\text{W/cm}^2) \times T (\text{s})$$

In reference [32], VABL performed 3600 s, and in reference [29], it performed 13,909 s of inactivation. The CSO generation on the corresponding CSO-time distribution (Fig. 10) was $128.8 \mu\text{M}$ and $127.2 \mu\text{M}$, respectively. The CSO concentrations in close quantities correspond to similar CFU reductions. It should be noted that these values were

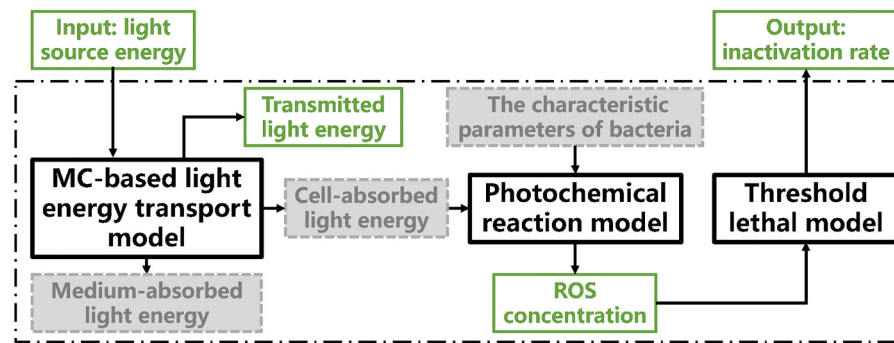


Fig. 11. Flow chart of the VABL inactivation model. The arrow directions indicate the input and output parameters of the model. The grey dashed boxes are internal parameters that cannot be measured directly, and the green solid boxes are parameters that can be obtained by experimental measurements. (For interpretation of the references to colour in this figure legend, the reader is referred to the web version of this article.)

obtained from the bacterial parameters defined in Appendix C and thus can only characterize relative magnitudes.

It can be inferred that, for a sparser SPR, less CSO is produced at the same light energy, and therefore, a higher light dose is required to achieve similar levels of inactivation. In practical applications such as wastewater treatment, more light energy than that used in the laboratory is needed, as the density of bacteria may be far sparser [50], so that the effectiveness of the deactivation is guaranteed.

For explaining the difference in the inactivation effect in the different mediums, our model also works. For *Listeria monocytogenes* inactivation, reference [51] achieved a $5.18 \log_{10}$ CFU reduction at a dose of 108 J/cm^2 (10 mW/cm^2), while reference [52] achieved a $3 \log_{10}$ CFU reduction at a dose of 1210 J/cm^2 ($7 \pm 2 \text{ mW/cm}^2$). The difference in the inactivation effect is mainly due to the medium in which the bacteria were exposed. The former experiment was carried out in a cell suspension, while the latter was performed on cantaloupe rinds. As analyzed above (Fig. 5(c) and Fig. 6(c)), the different mediums affect the light energy propagation. High doses are required in the reference [52] is because light is strongly absorbed or reflected on a solid medium. Therefore, in the case of sterilization in a medium where light energy propagation is obstructed, higher light energy is required to generate a lethal dose of singlet state oxygen.

The simulation results of CSO concentration are consistent with the fitted curves experimental results of the ROS concentration generated under VABL [16,53,54]. The simulation results appear to correspond to the experimental results in a linear relationship at low intensity for a shorter period. The convexity of the curve indicates that the rate of ROS generation decreases with increasing time. The experimental results showed that inactivation does not occur immediately upon light exposure [55]. The reason can be attributed to the fact that the accumulation rate may be equal to the self-scavenging rate of ROS [56,57] by bacterial cells. In our simulations, for deeper cells, little light energy can be absorbed, and thus, the concentration of singlet state oxygen produced was very low and may be cleared by the cells. Thus, the survival rate of bacteria is decreased after a period. Therefore, we deduce that a minimum threshold light intensity exists to achieve the desired inactivation effect. Furthermore, the photochemical reaction is unlikely to continue indefinitely. It is not clear exactly how long the reaction proceeds because the degree of tolerance of microorganisms to singlet state oxygen is unknown. Theoretically, the reaction stops when the ROS concentration is sufficient to cause cell death. The cell membrane or cell wall breaks down and the PS leaks to the external environment [58].

The marginal effects of light intensity on PS bleaching and CSO generation (Fig. 8) agree well the results given in references [59,60]. The light energy required to obtain the same reduction with increasing light intensity was investigated in reference [59]. The results showed that enhancing the light intensity reduces the reaction time but the dose required is increased for the same reductions. In reference [60], higher

light intensities were obtained by pulsed light. The relationship between light dose and inactivation is likely to be nonlinear, which corresponds to our simulation. We speculate that it can be attributed to the required time for the photochemical reaction. The primary photochemical reaction is the reaction of photons with PS. The secondary reaction is the conversion of triplet state oxygen to singlet state oxygen by PS. Increasing the light intensity can only increase the rate of the primary reaction, while the rate of the overall photochemical reaction will be limited by the secondary reaction.

As mentioned previously, VABL inactivation consists of two mechanisms. In this paper, we discussed only the accumulation process of singlet state oxygen due to its main toxicity in VABL inactivation. To describe the complete inactivation process more accurately, the type I reaction should also be considered in future work. In Appendix B, we give the reaction equations of type I ROS. However, type I reactions produce a variety of products, and it is difficult to directly detect the rate of product production, which is an urgent issue to be addressed in the future studies.

In the existing studies, the data on light source energy and inactivation rate are mainly provided. In fact, due to the excessive number of internal parameters included in the three processes (shown in Fig. 11), especially the characteristic parameters of bacteria, it is not yet possible to verify the model directly and precisely by existing data. More data need to be captured to apply our model. In the next step, we will validate the MC-based light energy transport model by measuring the relationship between scattered light and the light source energy. Based on this, we can obtain value of the light energy absorbed by the cells. Then, a series of real biological experiments will be carried out to build the dataset of the ROS concentration and the inactivation rate under different experimental conditions. The internal bacterial parameters can be fitter by the light energy absorbed by the cells and the produced ROS concentration. Finally, the threshold lethal model can establish a link between the ROS concentration and inactivation rate.

5. Conclusions

A Monte Carlo-based photon transport model with the optimized TTHG function was developed to obtain the ratio of cell-absorbed light energy, medium-absorbed light energy, and transmitted light energy in the light source energy. ELE-Depth distributions under different cell and medium parameters were shown. The kinetics of the photochemical reactions generating singlet state oxygen and the mathematical expressions for the intracellular PS and CSO concentrations were described. The distributions of CSO with time were obtained by simulating the dynamics of the VABL inactivation process in SPR according to the aforementioned model. The qualitative behavior of these distributions agreed well with the experimental results in existing studies. The correctness of our model is verified by using data from available

experiments. A series of real biological experiments will be carried out to build up the dataset to obtain accurate internal parameters. The reasons for the differences and similarities in VABL inactivation in different experiments can be explained from the perspective of light energy propagation by our work. The simulation results showed that when the cells were sparsely distributed, <30% of the light dose was absorbed. Therefore, it is inaccurate to use the electrical energy or intensity-meter-measured energy as the dose of participating photochemical reactions. The ELE-Depth distribution indicated that little light energy was available, and thus, the concentration of CSO produced was insufficient to inactivate microbes at deeper depths. The work in this paper can quantitatively calculate the singlet state oxygen distribution according to different experimental conditions. The model can provide more accurate light energy guidance for VABL inactivation, which will help promote the practical application of VABL and light source design.

CRediT authorship contribution statement

Wanqing Zhang: Methodology, Software, Writing – original draft.

Appendix A

Table 1
Definition and values of the parameters in PSO.

Parameter	Definition	Value
D	The dimension of solution space	3 (denoted a , g_a , g_b , respectively)
N	The number of particles	1000
U	The upper limit of iteration	100
ω_1	Inertia weight	decreases linearly from 0.9 to 0.4
c_1	The initial population learning factor	1.5
c_2	The initial individual learning factor	1.5

Appendix B

The original set of differential equations of the photochemical kinetics of VABL inactivation is defined by Eqs. (1)–(11). The type I reactions are described by Eqs. (1)–(3). The type II reactions are described by Eqs. (4)–(11) and generate CSO. Table 2 shows the definitions and units of the parameters used.

Type I:

$$\frac{d[O_2^-]}{dt} = (1 - S_\Delta)k_{oet}[^3O_2][e][T_1] - k_{oe}[O_2^-][e] \quad (1)$$

$$\frac{d[H_2O_2]}{dt} = k_{oe}[O_2^-][e] - k_{He}[H_2O_2][e] \quad (2)$$

$$\frac{d[HO^-]}{dt} = k_{He}[H_2O_2][e] - k_{AH}[A][HO^-] \quad (3)$$

Type II:

$$\frac{d[S_0]}{dt} = -k_0[S_0] + k_f[S_1] + k_p[T_1] + k_{ot}[T_1][^3O_2] - k_{os}\omega[S_0][^1O_2] \quad (4)$$

$$\frac{d[S_1]}{dt} = k_0[S_0] - k_f[S_1] - k_{isc}[S_1] = 0 \quad (5)$$

$$\frac{d[T_1]}{dt} = k_{isc}[S_1] - k_p[T_1] - k_{ot}[T_1][^3O_2] - k_{ta}[A][T_1] = 0 \quad (6)$$

$$\frac{d[^3O_2]}{dt} = -S_\Delta k_{ot}[T_1][^3O_2] + k_d[^1O_2] \quad (7)$$

$$\frac{d[^1O_2]}{dt} = S_\Delta k_{ot}[T_1][^3O_2] - k_d[^1O_2] - k_{oa}[A][^1O_2] - k_{os}\omega[S_0][^1O_2] = 0 \quad (8)$$

$$\frac{dA}{dt} = -k_{oa}[A][^1O_2] - k_{ta}[A][T_1] \quad (9)$$

Ping Su: Conceptualization, Data curation, Writing – review & editing.
Jianshe Ma: Conceptualization, Supervision, Funding acquisition.
Mali Gong: Conceptualization, Supervision.
Liya Ma: Software, Validation.
Jing Wang: Validation.

Declaration of Competing Interest

The authors declare that they have no known competing financial interests or personal relationships that could have appeared to influence the work reported in this paper.

Data availability

No data was used for the research described in the article.

Acknowledgement

This work was supported by the National Key Research and Development Program of China (Grant 2021YFB2802004).

$$k_0 = \frac{\sigma\phi}{h\nu} \quad (10)$$

$$\left[({}^1O_2)_{rx} \right] = fk_{oa}[A][{}^1O_2] - k_{ta}[A][T_1]dt \quad (11)$$

Table 2
Definitions and units of the parameters used to describe the photochemical equations.

Parameter	Definition	Units
$[O_2^-]$	Superoxide anion concentration	M
$[H_2O_2]$	Hydrogen peroxide concentration	M
$[HO^-]$	Hydroxyl radical concentration	M
$[S_0]$	Ground singlet state PS concentration	M
$[S_1]$	Excited singlet state PS concentration	M
$[T_1]$	Excited triplet state PS concentration	M
$[{}^3O_2]$	Triplet state oxygen concentration	M
$[{}^1O_2]$	Singlet state oxygen concentration	M
$[A]$	Molecular substrate concentration	M
$[e]$	Electron donor concentration	M
k_0	Photon absorption rate of PS per PS concentration	1/s
k_f	Decay rate of S_1 to ground state S_0	1/s
k_p	Decay rate of T_1	1/s
k_d	Decay rate of 1O_2 to 3O_2	1/s
k_{oe}	Bimolecular rate constant for reaction of O_2^- with e	1/Ms
k_{He}	Bimolecular rate constant for reaction of H_2O_2 with e	1/Ms
k_{AH}	Bimolecular rate constant for reaction of HO^- with A	1/Ms
k_{isc}	Decay rate of S_1 to T_1	1/Ms
k_{ot}	Bimolecular rate constant for reaction of 3O_2 with T_1	1/Ms
k_{os}	Bimolecular rate constant for reaction of 1O_2 with S_0	1/Ms
k_{oa}	Bimolecular rate constant for reaction of 1O_2 with A	1/Ms
k_{ta}	Bimolecular rate constant for reaction of T_1 with A	1/Ms
k_{oet}	Bimolecular rate constant for reaction of T_1 with e and 3O_2	1/M ² s
ω	Ratio of the actual PS to the initial value of the assumed PS	–
S_Δ	Fraction of T_1 and 3O_2 reactions that produce 1O_2	–
σ	Absorption cross section of S_0	cm ²
ϕ	Light intensity	W/cm ²
h	Planck constant	m ² kg/s
ν	Light frequency	m

Appendix C

Table 3 shows the definitions and units of the parameters used in Eqs. (6) and (7). Some of the values are taken from Lopez et al. [38].

Table 3
Definition and values of parameters.

Parameter	Definition	Value
β	k_p/k_{ot}	11.9 μM
γ	$k_{ta}[A]/k_{ot}$	23×10^{-6} μM
η	$k_{os}/k_{oa}[A]$	90×10^{-6} μM
κ	$[k_{isc}/(k_f + k_{isc})] \bullet (\sigma/h\nu)$	$23.3 \text{ cm}^2/\text{J}$
ξ	$S_\Delta \bullet \kappa/(1 + k_d/k_{oa}A)$	$21 \text{ cm}^2/\text{J}$
$({}^3O_2)_0$	Constant; ambient oxygen	80 μM
S_{00}	Initial value of S_0	40 μM
Φ	Light intensity	obtained by MC (W/cm ²)
ω	(See Table. 2)	$\omega \geq 1$; $\omega = 1$ in this paper
S_Δ	(See Table. 2)	$S_\Delta \leq 1$; $S_\Delta = 0.8$ in this paper [16]
f	Reaction ratio	$f \leq 1$; $f = 0.1$ in this paper

References

- [1] C.P. Sabino, et al., Light-based technologies for management of COVID-19 pandemic crisis, *J. Photochem. Photobiol. B* 212 (Nov. 2020) 111999, <https://doi.org/10.1016/j.jphotobiol.2020.111999>.
- [2] C.S. Enwemeka, V.V. Burnah, D.S. Masson-Meyers, Light as a potential treatment for pandemic coronavirus infections: a perspective, *J. Photochem. Photobiol. B* 207 (Jun. 2020) 111891, <https://doi.org/10.1016/j.jphotobiol.2020.111891>.
- [3] E. O'Flaherty, J.-M. Membré, E. Cummins, Meta-analysis of the reduction of antibiotic-sensitive and antibiotic-resistant Escherichia coli as a result of low- and medium-pressure UV lamps, *Water Sci. Technol.* 2017 (2) (May 2018) 612–620, <https://doi.org/10.2166/wst.2018.183>.
- [4] M. Maclean, K. McKenzie, J.G. Anderson, G. Gettinby, S.J. MacGregor, 405 nm light technology for the inactivation of pathogens and its potential role for environmental disinfection and infection control, *J. Hosp. Infect.* 88 (1) (Sep. 2014) 1–11, <https://doi.org/10.1016/j.jhin.2014.06.004>.

- [5] L.G. Leanse, C. dos Anjos, S. Mushtaq, T. Dai, Antimicrobial blue light: a ‘magic bullet’ for the 21st century and beyond? *Adv. Drug Deliv. Rev.* 180 (Jan. 2022) 114057, <https://doi.org/10.1016/j.addr.2021.114057>.
- [6] M.R. Hamblin, H. Abrahamse, Oxygen-independent antimicrobial Photoinactivation: type III photochemical mechanism? *Antibiotics* 9 (2) (Jan. 2020) 53, <https://doi.org/10.3390/antibiotics9020053>.
- [7] V. Plavskii, et al., Porphyrins and flavins as endogenous acceptors of optical radiation of blue spectral region determining photoinactivation of microbial cells, *J. Photochem. Photobiol. B* 183 (2018) 172–183, <https://doi.org/10.1016/j.jphotobiol.2018.04.021>.
- [8] Y. Wang, et al., Antimicrobial blue light inactivation of pathogenic microbes: state of the art, *Drug Resist. Updat. Rev. Comment. Antimicrob. Anticancer Chemother.* 33–35 (2017) 1–22, <https://doi.org/10.1016/j.drup.2017.10.002>.
- [9] M.-J. Kim, M. Mikš-Krajnik, A. Kumar, V. Ghate, H.-G. Yuk, Antibacterial effect and mechanism of high-intensity $405\pm5\text{nm}$ light emitting diode on *Bacillus cereus*, *Listeria monocytogenes*, and *Staphylococcus aureus* under refrigerated condition, *J. Photochem. Photobiol. B* 153 (Dec. 2015) 33–39, <https://doi.org/10.1016/j.jphotobiol.2015.08.032>.
- [10] Y. Wang, R. Ferrer-Espada, Y. Baglo, Y. Gu, T. Dai, Antimicrobial blue light inactivation of *Neisseria gonorrhoeae*: roles of wavelength, endogenous photosensitizer, oxygen, and reactive oxygen species, *Lasers Surg. Med.* 51 (9) (Nov. 2019) 815–823, <https://doi.org/10.1002/lsm.23104>.
- [11] M. Maclean, S.J. MacGregor, J.G. Anderson, G.A. Woolsey, The role of oxygen in the visible-light inactivation of *Staphylococcus aureus*, *J. Photochem. Photobiol. B* 92 (3) (Sep. 2008) 180–184, <https://doi.org/10.1016/j.jphotobiol.2008.06.006>.
- [12] R.M. Tomb, M. Maclean, P.R. Herron, P.A. Hoskisson, S.J. MacGregor, J. G. Anderson, Inactivation of *Streptomyces* phage φC31 by 405 nm light: requirement for exogenous photosensitizers? *Bacteriophage* 4 (3) (Jul. 2014), e32129 <https://doi.org/10.4161/bact.32129>.
- [13] M.S. Baptista, et al., Type I and type II photosensitized oxidation reactions: guidelines and mechanistic pathways, *Photochem. Photobiol.* 93 (4) (Jul. 2017) 912–919, <https://doi.org/10.1111/php.12716>.
- [14] P. Di Mascio, G.R. Martínez, S. Miyamoto, G.E. Ronsein, M.H.G. Medeiros, J. Cadet, Singlet molecular oxygen reactions with nucleic acids, lipids, and proteins, *Chem. Rev.* 119 (3) (Feb. 2019) 2043–2086, <https://doi.org/10.1021/acs.chemrev.8b00554>.
- [15] L.G. Leanse, X. Zeng, T. Dai, Potentiated antimicrobial blue light killing of methicillin resistant *Staphylococcus aureus* by pyocyanin, *J. Photochem. Photobiol. B* 215 (Feb. 2021) 112109, <https://doi.org/10.1016/j.jphotobiol.2020.112109>.
- [16] T. Wang, J. Dong, G. Zhang, Analysis and data-based modeling of the photochemical reaction dynamics of the induced singlet oxygen in light therapies, *IEEE Trans. Biomed. Eng.* 69 (11) (Nov 2022) 3427–3437, <https://doi.org/10.1109/TBME.2022.3170541>.
- [17] S.E. Baché, et al., Clinical studies of the high-intensity narrow-Spectrum light environmental decontamination system (HINS-light EDS), for continuous disinfection in the burn unit inpatient and outpatient settings, *Burns* 38 (1) (Feb. 2012) 69–76, <https://doi.org/10.1016/j.burns.2011.03.008>.
- [18] S.E. Baché, M. Maclean, G. Gettinby, J.G. Anderson, S.J. MacGregor, I. Taggart, Universal decontamination of hospital surfaces in an occupied inpatient room with a continuous 405 nm light source, *J. Hosp. Infect.* 98 (1) (Jan. 2018) 67–73, <https://doi.org/10.1016/j.jhin.2017.07.010>.
- [19] M. Cossu, L. Ledda, A. Cossu, Emerging trends in the photodynamic inactivation (PDI) applied to the food decontamination, *Food Res. Int.* 144 (Jun. 2021) 110358, <https://doi.org/10.1016/j.foodres.2021.110358>.
- [20] Y. Wang, et al., Antimicrobial Blue Light Inactivation of Gram-Negative Pathogens in Biofilms: In Vitro and In Vivo Studies, *J. Infect. Dis.* 213 (9) (2016) 1380–1387, <https://doi.org/10.1093/infdis/jiw070>.
- [21] L.G. Leanse, X.S. Goh, J.-X. Cheng, D.C. Hooper, T. Dai, Dual-wavelength photo-killing of methicillin-resistant *Staphylococcus aureus*, *JCI Insight* 5 (11) (Jun. 2020), <https://doi.org/10.1172/jci.insight.134343>.
- [22] Y. Zhang, et al., Antimicrobial blue light therapy for multidrug-resistant *Acinetobacter baumannii* infection in a mouse burn model: implications for prophylaxis and treatment of combat-related wound infections, *J. Infect. Dis.* 209 (12) (Jun. 2014) 1963–1971, <https://doi.org/10.1093/infdis/jit842>.
- [23] E.J. Cotter, et al., Efficacy of combinational therapy using blue light and benzoyl peroxide in reducing *Cutibacterium acnes* bioburden at the deltopectoral interval: a randomized controlled trial, *J. Shoulder Elb. Surg.* 30 (12) (Dec. 2021) 2671–2681, <https://doi.org/10.1016/j.jse.2021.08.008>.
- [24] D.-K. Kim, D.-H. Kang, Efficacy of light-emitting diodes emitting 395, 405, 415, and 425 nm blue light for bacterial inactivation and the microbicidal mechanism, *Food Res. Int.* 141 (Mar. 2021), 110105, <https://doi.org/10.1016/j.foodres.2021.110105>.
- [25] K. Hoenes, R. Bauer, T. Meurle, B. Spellerberg, M. Hessling, Inactivation effect of violet and blue light on ESKAPE pathogens and closely related non-pathogenic bacterial species – a promising tool against antibiotic-sensitive and antibiotic-resistant microorganisms, *Front. Microbiol.* 11 (2020), <https://doi.org/10.3389/fmicb.2020.612367>.
- [26] T.L. Vollmerhausen, A. Conneely, C. Bennett, V.E. Wagner, J.C. Victor, C. P. O’Byrne, Visible and UVA light as a potential means of preventing *Escherichia coli* biofilm formation in urine and on materials used in urethral catheters, *J. Photochem. Photobiol. B* 170 (May 2017) 295–303, <https://doi.org/10.1016/j.jphotobiol.2017.04.018>.
- [27] J. Marugán, R. van Grieken, C. Sordo, C. Cruz, Kinetics of the photocatalytic disinfection of *Escherichia coli* suspensions, *Appl. Catal. B Environ.* 82 (1–2) (Jul. 2008) 27–36, <https://doi.org/10.1016/j.apcatb.2008.01.002>.
- [28] C.P. Sabino, et al., Inactivation kinetics and lethal dose analysis of antimicrobial blue light and photodynamic therapy, *Photodiagn. Photodyn. Ther.* 28 (Dec. 2019) 186–191, <https://doi.org/10.1016/j.pdptd.2019.08.022>.
- [29] A. Kumar, V. Ghate, M.-J. Kim, W. Zhou, G.H. Khoo, H.-G. Yuk, Kinetics of bacterial inactivation by 405nm and 520nm light emitting diodes and the role of endogenous coproporphyrin on bacterial susceptibility, *J. Photochem. Photobiol. B* 149 (Aug. 2015) 37–44, <https://doi.org/10.1016/j.jphotobiol.2015.05.005>.
- [30] R.M. Valentine, C.T.A. Brown, H. Moseley, S. Ibbotson, K. Wood, Monte Carlo modeling of in vivo protoporphyrin IX fluorescence and singlet oxygen production during photodynamic therapy for patients presenting with superficial basal cell carcinomas, *J. Biomed. Opt.* 16 (4) (2011), 048002, <https://doi.org/10.1117/1.3562540>.
- [31] C.L. Campbell, K. Wood, R.M. Valentine, C.T.A. Brown, H. Moseley, Monte Carlo modelling of daylight activated photodynamic therapy, *Phys. Med. Biol.* 60 (10) (May 2015) 4059–4073, <https://doi.org/10.1088/0031-9155/60/10/4059>.
- [32] M. Maclean, S.J. MacGregor, J.G. Anderson, G. Woolsey, Inactivation of bacterial pathogens following exposure to light from a 405-nanometer light-emitting diode Array, *Appl. Environ. Microbiol.* 75 (7) (Apr. 2009) 1932–1937, <https://doi.org/10.1128/AEM.01892-08>.
- [33] M. Maclean, et al., Non-ionizing 405 nm light as a potential bactericidal Technology for Platelet Safety: evaluation of in vitro bacterial inactivation and in vivo platelet recovery in severe combined Immunodeficient mice, *Front. Med.* 6 (Jan. 2020) 331, <https://doi.org/10.3389/fmed.2019.00331>.
- [34] K.I. Jankowska, et al., Complete inactivation of blood borne pathogen *Trypanosoma cruzi* in stored human platelet concentrates and plasma treated with 405 nm violet-blue light, *Front. Med.* 7 (Nov. 2020) 617373, <https://doi.org/10.3389/fmed.2020.617373>.
- [35] M.-J. Kim, M. Da Jeong, Q. Zheng, H.-G. Yuk, Antimicrobial activity of 405 nm light-emitting diode (LED) in the presence of riboflavin against *Listeria monocytogenes* on the surface of smoked salmon, *Food Sci. Biotechnol.* 30 (4) (Apr. 2021) 609–618, <https://doi.org/10.1007/s10068-021-00895-y>.
- [36] G.J. Tortora, B.R. Funke, C.L. Case, *Microbiology: An Introduction*, 10th ed., Pearson Benjamin Cummings, San Francisco, CA, 2010.
- [37] J.M. Willey, L. Sherwood, C.J. Woolverton, *Prescott’s Microbiology*, Ninth edition, McGraw-Hill, New York, NY, 2014.
- [38] N. Lopez, R. Mulet, R. Rodríguez, Tumor reactive ringlet oxygen approach for Monte Carlo modeling of photodynamic therapy dosimetry, *J. Photochem. Photobiol. B* 160 (Jul. 2016) 383–391, <https://doi.org/10.1016/j.jphotobiol.2016.04.014>.
- [39] L. Wang, S.L. Jacques, L. Zheng, MCML—Monte Carlo modeling of light transport in multi-layered tissues, *Comput. Methods Prog. Biomed.* 47 (2) (Jul. 1995) 131–146, [https://doi.org/10.1016/0169-2607\(95\)01640-F](https://doi.org/10.1016/0169-2607(95)01640-F).
- [40] S.K. Sharma, A.A. Kokhanovsky, A review of approximate analytic light-scattering phase functions, in: *Light Scattering Reviews 9*, Springer Berlin Heidelberg, Berlin, Heidelberg, 2015, pp. 53–100, https://doi.org/10.1007/978-3-642-37985-7_2.
- [41] A.C. Selden, Attenuation and impulse response for multiple scattering of light in atmospheric clouds and aerosols, *Appl. Opt.* 45 (13) (May 2006) 3144, <https://doi.org/10.1364/AO.45.003144>.
- [42] C.B. Honsberg, S.G. Bowden, Absorption Coefficient, page on, <http://www.pveducation.org>, 2019, <https://www.pveducation.org/pvcdrom/welcome-to-pvcdrom/instructions>.
- [43] L. do Prado-Silva, G.T.P. Brancini, G.Ú.L. Braga, X. Liao, T. Ding, A.S. Sant’Ana, Antimicrobial photodynamic treatment (aPDT) as an innovative technology to control spoilage and pathogenic microorganisms in Agri-food products: an updated review, *Food Control* 132 (Feb. 2022), 108527, <https://doi.org/10.1016/j.foodcont.2021.108527>.
- [44] M. Ochsner, Photophysical and photobiological processes in the photodynamic therapy of tumours, *J. Photochem. Photobiol. B* 39 (1) (May 1997) 1–18, [https://doi.org/10.1016/S1011-1344\(96\)07428-3](https://doi.org/10.1016/S1011-1344(96)07428-3).
- [45] B. Liu, T.J. Farrell, M.S. Patterson, A dynamic model for ALA-PDT of skin: simulation of temporal and spatial distributions of ground-state oxygen, photosensitizer and singlet oxygen, *Phys. Med. Biol.* 55 (19) (Oct. 2010) 5913–5932, <https://doi.org/10.1088/0031-9155/55/19/019>.
- [46] C.L. Campbell, K. Wood, C.T.A. Brown, H. Moseley, New insights into photodynamic therapy treatment through the use of 3D Monte Carlo radiation transfer modelling, in: Presented at the SPIE BiO, San Francisco, California, United States, Feb 2016, p. 9689Q, <https://doi.org/10.1117/12.2212240>.
- [47] C. dos Anjos, et al., Inactivation of milk-borne pathogens by blue light exposure, *J. Dairy Sci.* 103 (2) (Feb. 2020) 1261–1268, <https://doi.org/10.3168/jds.2019-16758>.
- [48] C.F. Stewart, et al., Violet-blue 405-nm light-based Photoinactivation for pathogen reduction of human plasma provides broad antibacterial efficacy without visible degradation of plasma proteins, *Photochem. Photobiol.* 98 (2) (Mar. 2022) 504–512, <https://doi.org/10.1111/php.13584>.
- [49] X. Wang, X. Hu, H. Wang, C. Hu, Synergistic effect of the sequential use of UV irradiation and chlorine to disinfect reclaimed water, *Water Res.* 46 (4) (Mar. 2012) 1225–1232, <https://doi.org/10.1016/j.watres.2011.12.027>.
- [50] L.E. Murdoch, M. Maclean, E. Endarko, S.J. MacGregor, J.G. Anderson, Bactericidal effects of 405 nm light exposure demonstrated by inactivation of *Escherichia, Salmonella, Shigella, Listeria, and Mycobacterium* species in liquid suspensions and on exposed surfaces, *Sci. World J.* 2012 (2012) 1–8, <https://doi.org/10.1100/2012/137805>.
- [51] S.W. Josewin, M.-J. Kim, H.-G. Yuk, Inactivation of *Listeria monocytogenes* and *Salmonella* spp. on cantaloupe rinds by blue light emitting diodes (LEDs), *Food Microbiol.* 76 (Dec. 2018) 219–225, <https://doi.org/10.1016/j.fm.2018.05.012>.

- [53] J. Dong, T. Wang, Data driven modeling of the reactive oxygen species stimulated by photon energy in light therapies, *IEEE Access* 8 (2020) 18196–18206, <https://doi.org/10.1109/ACCESS.2020.2968352>.
- [54] T. Wang, J. Dong, G. Zhang, Analyzing efficacy and safety of anti-fungal blue light therapy via kernel-based modeling the reactive oxygen species induced by light, *IEEE Trans. Biomed. Eng.* 69 (8) (2022 Aug) 2433–2442, <https://doi.org/10.1109/TBME.2022.3146567>.
- [55] T. Wang, J. Dong, H. Yin, G. Zhang, Blue light therapy to treat candida vaginitis with comparisons of three wavelengths: an in vitro study, *Lasers Med. Sci.* 35 (6) (Aug. 2020) 1329–1339, <https://doi.org/10.1007/s10103-019-02928-9>.
- [56] E. Cadenas, Biochemistry of oxygen toxicity, *Annu. Rev. Biochem.* 58 (1) (Jun. 1989) 79–110, <https://doi.org/10.1146/annurev.bi.58.070189.000455>.
- [57] H. Yamasaki, H. Uefuji, Y. Sakihama, Bleaching of the red anthocyanin induced by superoxide radical, *Arch. Biochem. Biophys.* 332 (1) (Aug. 1996) 183–186, <https://doi.org/10.1006/abbi.1996.0331>.
- [58] R. Nguenha, et al., Effect of photosensitization mediated by curcumin on carotenoid and aflatoxin content in different maize varieties, *Appl. Sci.* 11 (13) (Jun. 2021) 5902, <https://doi.org/10.3390/app11135902>.
- [59] F. Chen, X. Yang, Q. Wu, Photocatalytic oxidation of escherichia coli, aspergillus niger, and formaldehyde under different ultraviolet irradiation conditions, *Environ. Sci. Technol.* 43 (12) (Jun. 2009) 4606–4611, <https://doi.org/10.1021/es900505h>.
- [60] J.B. Gillespie, et al., Efficacy of pulsed 405-nm light-emitting diodes for antimicrobial photodynamic inactivation: effects of intensity, frequency, and duty cycle, *Photomed. Laser Surg.* 35 (3) (Mar. 2017) 150–156, <https://doi.org/10.1089/pho.2016.4179>.